The Influence of Cross-Sectional Shape and Orientation of Micropillar Surface on Microdroplet Formation by a Dewetting Process

Bambang Arip Dwiyantoro[1] & Shiu-Wu Chau[2]

[1]Department of Mechanical Engineering, Institute of Technology Sepuluh Nopember, Kampus ITS, Sukolilo, Surabaya 60111, Indonesia
[2]Department of Mechanical Engineering, National Taiwan University of Science and Techonology, Keelung Road Sec. 4, Taipei 106, Taiwan
Email: bambangads@me.its.ac.id

Abstract. In this study the dewetting process on micropillars of three different cross-sectional shapes, i.e. circular, square and triangular, was numerically investigated. The influence of the orientation of the triangular and square micropillars on the dewetting behavior was also studied. The numerical simulations showed that the cross-sectional shapes of the micropillars and their orientation play an important role in determining the flow pattern of the dewetting process, especially the evolution and movement of the meniscus across the micropillar before a microdroplet is formed. The diameter of the microdroplets is mainly determined by the capillary effect, viscous drag and fluid inertia contributed by the peeling rate and the thickness of the water layer above the micropillar. The numerical results also indicate that the hydraulic diameter of the micropillars (Dp) is one of the parameters governing the size of the microdroplets formed on the top surface of the micropillars after the dewetting process, while the microdroplet diameter is almost insensitive to the cross-sectional shape and orientation of the micropillars. The dimensionless diameter of the microdroplets (d) can then be expressed as a function of a dimensionless group, i.e. the Ohnesorge number (Oh), the capillary number (Ca), the dimensionless liquid thickness (H), and the contact angle (θ).

Keywords: *cross-sectional shapes; dewetting process; diameter; microdroplet; numerical; orientation of micropillar.*

1 Introduction

In recent years, the generation of microdroplets on solid surfaces through dewetting has received great attention in many scientific and engineering applications. Sugiura, *et al.* [1] have performed an experimental investigation of droplets in microchannels, where the droplet size is determined by the microchannel geometry, i.e. the microchannel depth and terrace length. Xu, *et al.* [2] experimentally conducted droplet formation from a micrometer screen

Received December 3rd, 2012, Revised April 2nd, 2013, Accepted for publication May 14th, 2013.
 ISSN: 2337-5779, DOI: 10.5614/j.eng.technol.sci.2013.45.2.5

hole. They found that the flow rate had little influence on the droplet size. Gupta and Kumar [3] studied the effects of T-junction geometry on droplet formation using three-dimensional lattice Boltzmann simulations. Luo, *et al.* [4] created droplets on stripe-patterned substrates by thin polymer film dewetting. They examined the influence of different dewetting processes on the formation of polygonal liquid droplets. Mulji and Chandra [5] researched the rupture and dewetting of water films on solid surfaces with materials of various wettability and roughness. They disclosed how a liquid film ruptures when it is spread on a surface that is not ideally smooth. Yoon, *et al.* [6] observed microstructures of polymer thin films on topographically pre-patterned substrates based on a controlled dewetting of films. Their results show that the pattern formations were determined by the geometry and morphology of the dewetted polymer films. Zhang, *et al.* [7] researched how to form regular polymer microstructures by dewetting thin polymer film. They disclosed a fast and reproducible process that can pattern thin polymer film at micrometer scale by direct dewetting. Martin, *et al.* [8] studied pattern formation of nanoparticle assemblies by solvent dewetting. They discussed the dependence of nanoparticle size on surface properties. Reiter, *et al.* [9] investigated the evolution of the shape of the dewetting rim. They argued that dewetting represents a powerful approach for the characterization of the interfacial properties of thin polymer films. Karthaus, *et al.* [10] studied droplet size and spacing in a micrometer-sized polymeric dewetting process. They examined the effects of polymer concentration and roller speed on the diameter of polymer microdroplets and their lateral spacing.

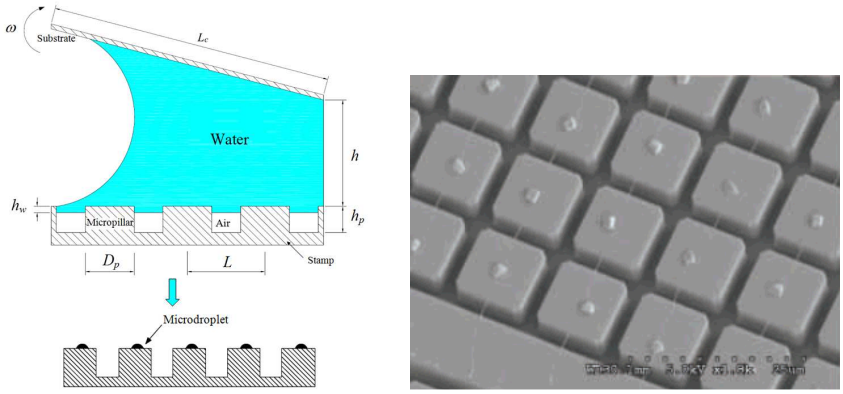

Figure 1 (a) Schematic illustration of an experimental procedure for the generation of microdroplets. (b) Image of microdroplets left on micropillar stamps [11].

In a previous study of the authors [12], a microdroplet array was successfully created on a micropillar-featured surface and also the corresponding dewetting process as modeled using a numerical approach, where the mechanism for the formation of the microdroplets on the columns of the micropillars was clarified as well. It was also demonstrated that the size of the nanoparticles created after evaporation of the fluid was controlled by the volume of the microdroplets and the concentration of the solution. Figure 1 shows a schematic illustration of the experimental procedure to generate the microdroplet array adopted in our previous work. The generation of microdroplets is easily achieved by gently placing a stamp featured with a micropillar structure onto a small droplet of solution relocated on the substrate and then peeling it up.

The objective of this work was to investigate the influence of three different cross-sectional shapes and their orientation on dewetting behavior. The correlation between the diameter of the microdroplets and the parameters governing the dewetting process on the micropillar array will also be discussed.

2 Mathematical Model and Numerical Method

The dewetting process on micropillars discussed in this paper can be described as the evolution of a receding water meniscus located between two solid, horizontally parallel surfaces, caused by rotation of the upper one. Figure 1(a) schematically illustrates the geometry of the micropillars, where D_p represents the hydraulic diameter of the micropillars, h_p the height of the micropillars, L the center to center distance between the micropillars, L_c the length of the upper substrate, h the liquid thickness between the top surface of the micropillars and the upper substrate, h_w the water submergence depth between the micropillars, and ω the peeling speed of the upper substrate.

The first two governing equations to describe the front-moving flow, i.e. the continuity equation and the Navier-Stokes equation, can be expressed in the integral form over a control volume V as follows:

$$\frac{\mathrm{d}}{\mathrm{d}t}\int_V \rho \mathrm{d}V + \int_S \rho(\mathbf{v}-\mathbf{v}_S)\cdot \mathrm{d}S = 0 \tag{1}$$

$$\frac{\mathrm{d}}{\mathrm{d}t}\int_V \rho \mathbf{v} \mathrm{d}V + \int_S \rho \mathbf{v}(\mathbf{v}-\mathbf{v}_S)\cdot \mathrm{d}S = \int_S \mathbf{f}\mathrm{d}S + \int_V \rho \mathbf{g}\mathrm{d}V \tag{2}$$

where the control volume V is bounded by a closed surface S, $\mathbf{v}$ denotes the flow velocity, $\mathbf{v}_S$ the surface velocity of S, ρ the fluid density, t the time, $\mathbf{f}$ the

external force acting on *S*, and **g** the gravitational acceleration. The surface force **f** is computed as follows:

$$f_i = \mu\left(\frac{\partial v_i}{\partial x_j} + \frac{\partial v_j}{\partial x_i}\right)e_j - pe_i + f_i^{\sigma} \tag{3}$$

where v_i denotes the velocity component in the direction of the Cartesian coordinate x_i with the unit vector of e_i, and f_i^{σ} denotes the component of surface tension in the direction of x_i, μ the viscosity, and p the pressure. The surface velocity $\mathbf{v}_S$ is then determined by the third governing equation in order to avoid errors caused by the direct calculation of the surface velocity of the cell-face center displacement:

$$\frac{\mathrm{d}}{\mathrm{d}t}\int_V \mathrm{d}V + \int_S \mathbf{v}_S \cdot \mathrm{d}S = 0 \tag{4}$$

The last governing equation, employed as follows, is to describe the position of the water front:

$$\frac{\mathrm{d}}{\mathrm{d}t}\int_V c\mathrm{d}V + \int_S c(\mathbf{v} - \mathbf{v}_S)\cdot \mathrm{d}S = 0 \tag{5}$$

where c represents the volume fraction of the fluid, i.e. $c = 0$ for cells filled with air and the case of $0 < c < 1$ for cells filled with both fluids and $c = 1$ for cells filled with liquid (water).

The numerical scheme used to solve these coupled governing equations was based on a finite volume discretization. All vector quantities, e.g. vector position, velocity and moment of momentum, were expressed in Cartesian coordinates. A non-staggered variable arrangement was used to define the dependent variables: all physical quantities were stored and computed at the cell center. An interpolation practice of second-order accuracy was as adopted to calculate the field variables at the center of the cell-face [13]. The deferred correction approach, proposed by Khosla and Rubin [14], was used to calculate the convection term by blending the upwind and central difference schemes. The diffusion terms were approximated by the central difference scheme with second-order accuracy, while the gradient of field variable was calculated in the same manner as that for the cell-face center. Finally, the SIMPLE algorithm proposed by Patankar [15] was adopted to separate the coupling between velocity and pressure. Details of the mathematical model and the numerical scheme can be found in our previous work [16].

In this study water was employed as the working fluid, where the water properties were ρ = 998.3 kg/m^3, the viscosity μ = 1.002×10^{-3} N s/m^2, and the surface tension σ = 0.074 N/m, while the air properties were ρ = 1.188 kg/m^3, μ = 1.824×10^{-5} N s/m^2. In numerical simulations of the dewetting process on a micropillar surface, the geometric characteristics of the micropillars are given based on the diameter of the micropillars (D_p), i.e. h_p = 0.5 D_p, and h_w = 0.1 D_p. For non-circular micropillars, the hydraulic diameter (D_h) is adopted to characterize the size of the micropillars instead of D_p. The value of h_w has little influence on the size of the microdroplets, provided it does not exceed a critical depth [12]. The typical grid adopted in the numerical simulation was 0.7×10^6 hexahedral cells to discretize the computational domain for a row array arrangement consisting of five micropillars, see Figure 2. A body-fitted grid was employed to describe the flow space, which was regenerated at every time step to exactly match the computational domain defined by the peeling movement of the upper surface. The liquid-gas meniscus was tracked by an interface-capturing approach in which the numerical grid extended over both liquids and the front was implicitly defined by location of volume fraction equals 0.5. The typical time step used in our numerical simulations was in tens of nanoseconds to ensure the required numerical stability. Figure 3 shows the droplet volume (V_d) for the case of D_p = 7 μm and ω = 10 rad/s with eight successively refined grids. The dash-dot line is the grid-independent solution estimated using the Richardson's extrapolation [17]. For the typical grid, the discretization error was less than about 1.6%.

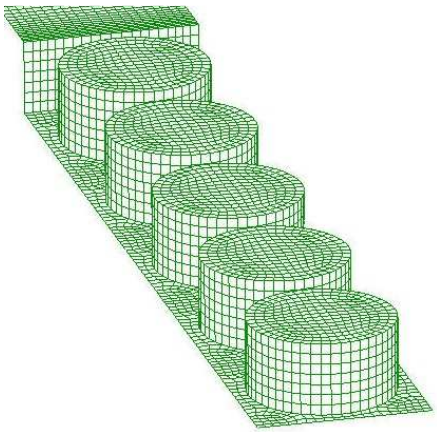

Figure 2 Numerical grid employed in the simulation of the dewetting process on circular micropillars.

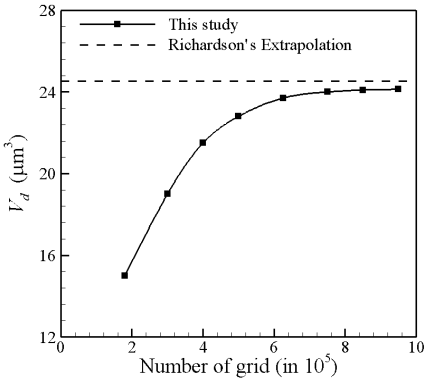

Figure 3 Droplet volume (V_d) as a function of grid number for the case of D_p = 7 μm and ω = 10 rad/s.

3 Results and Discussion

Figure 4 shows the evolution of the water front moving across the circular micropillars with D_p = 7 μm and ω = 10 rad/s, where t = 0 denotes the moment at which the peeling starts. The dewetting occurs from the edge of the top surface of the micropillars and results in an island-like fluid region behind the main front. The island-like region finally detaches itself from the main front because of surface tension. The fluid remaining on the column of the micropillars lowers its velocity because of viscous damping of the contact surface. After the recoiling of the captive wet region, a droplet is formed on top of the micropillar.

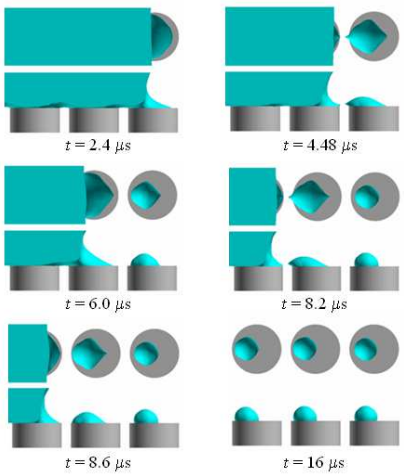

Figure 4 Time evolution of the water front moving across circular micropillars.

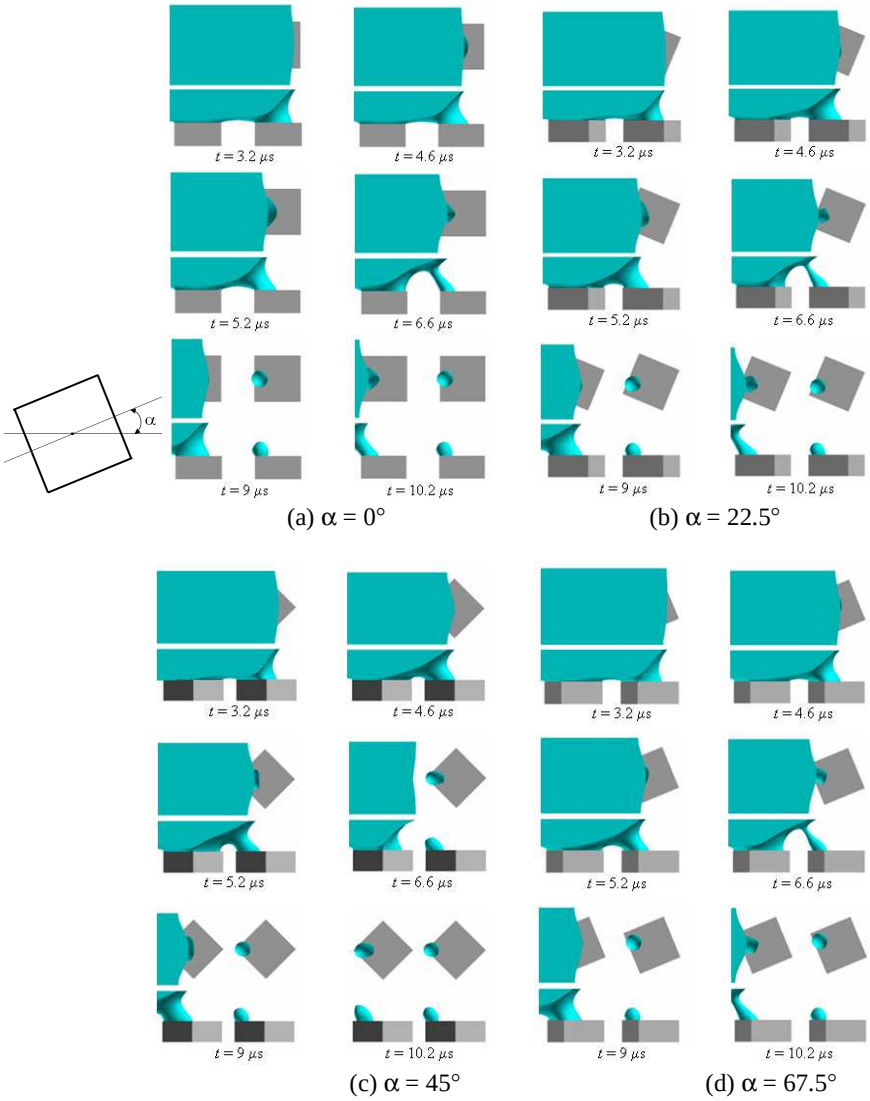

Figure 5 Dewetting on the top surface of square micropillars.

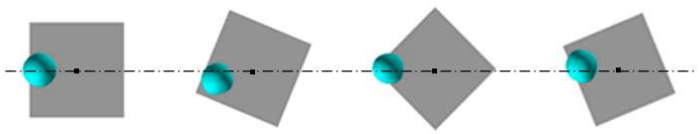

(a) α = 0° (b) α = 22.5° (c) α = 45° (d) α = 67.5°

Figure 6 Final positions of microdroplets on the top surface of square micropillars.

The diameter of the droplets is mainly determined by the contribution of capillary, viscous, and inertia forces. The volume of a microdroplet V_d was employed to calculate the effective diameter of a microdroplet (D), as follows:

$$D = \sqrt[3]{\frac{6V_d}{\pi}} \tag{6}$$

Dewetting simulations on square and triangular micropillars at different orientations, with α denoting the orientation angle, were conducted to disclose the influences of the cross-sectional shape and its orientation on the dewetting process. Figure 5 gives the evolution of the water front moving across square micropillars for D_h = 7 μm and ω = 10 rad/s with four different orientations, i.e. α = 0°, 22.5°, 45°, and 67.5°. A different orientation leads to similar flow patterns but results in detachment times of the microdroplets. The square micropillar at α = 45° gives the shortest detachment time from the four different orientations because it has the most streamlined outline in the aft part, while the square micropillar with α = 0° has the longest detachment time because it has the most blunt outline in the aft part. Figure 6 illustrates the final position of the microdroplet on the top surface of a square micropillar at different orientations. The microdroplet is prone to stay near the far edge on the top surface along the peeling direction, except when two symmetrical far edges exist.

Figure 7 depicts the evolution of the water front moving across triangular micropillars for D_h = 7 μm and ω =10 rad/s with four orientations, i.e. α = 0°, 30°, 60°, and 90°. Compared to the cases with square micropillars, the triangular micropillars show a similar dewetting behavior. The simulation results for triangular micropillars again highlight the influence of the aft-part shape on the detachment time. The triangular micropillar with α = 60° yields the shortest detachment time, and the triangular micropillar with α = 0° shows the longest detachment time. Figure 8 demonstrates the influence of orientation

on the final position of the microdroplet on the top surface of a triangular micropillar.

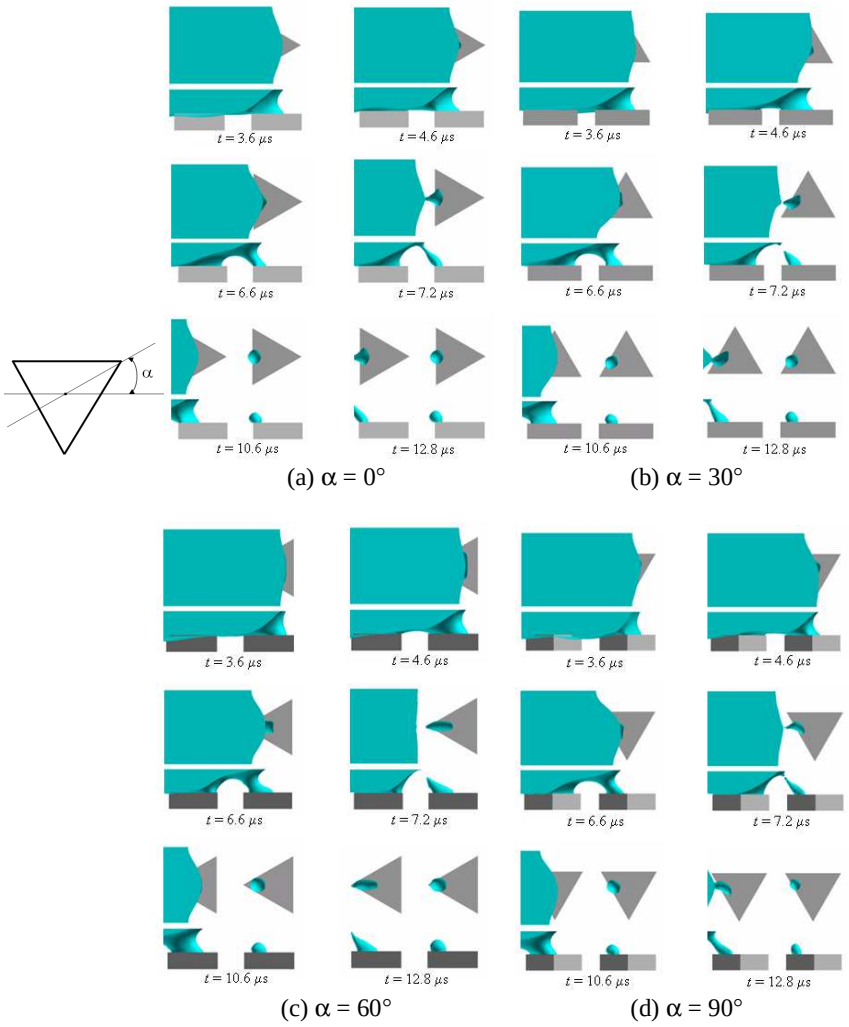

Figure 7 Dewetting on the top surface of triangular micropillars.

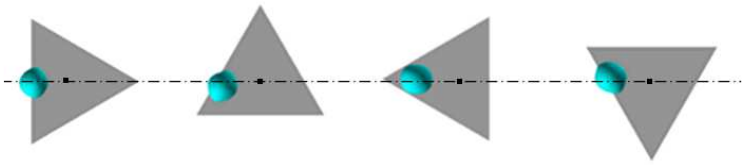

(a) α = 0° (b) α = 30° (c) α = 60° (d) α = 90°

Figure 8 Final positions of microdroplets on the top surface of triangular micropillars.

The diameter of microdroplets left on the top surface of micropillars can be expressed as a function of the geometry of the micropillar, fluid properties, and peeling speed:

$$D = f\left(D_p, h, \omega, L_c, L, \rho, \mu, \sigma, \theta\right) \tag{7}$$

With the help of a dimensional analysis, the dimensionless diameter of microdroplet (d) depends on the following dimensionless group:

$$d = f\left(\mathrm{Oh}, \mathrm{Ca}, H, \theta\right) \tag{8}$$

where $d = D/D_p$, $\mathrm{Oh} = \mu/(\rho\sigma D_p)^{1/2}$, $\mathrm{Ca} = \mu L_c\omega/\sigma$, $H = h/D_p$, and θ denotes the contact angle. The contact angle is formed between the solid surface and the tangent to a collapsing family of isodensity curves far away from it. This contact angle is found to increase almost linearly with the capillary number. The influence of L on the magnitude of the droplet diameter in a linear arrangement is negligible [18]. In our simulations, the change in the Ohnesorge number (Oh) was determined by the choice of D_p, while the variation in the capillary number (Ca) was governed by the selection of ω.

Figure 9 represents the dependence of the dimensionless droplet diameter (d) on the dimensionless liquid thickness (H) at $\mathrm{Oh} = 4.39\times10^{-2}$ and $\mathrm{Ca} = 7.43\times10^{-4}$. The dimensionless microdroplet diameter varies little compared to the cross-sectional shape with the same size of D_h. The size of the droplet is also almost insensitive to the orientation of the micropillar. The numerical results suggest that the dimensionless microdroplet diameter is not a function of the cross-sectional shape and orientation of the micropillar. This indicates that the cross-sectional shape and orientation of the micropillar can only enhance the hysteresis effect of the water front as it moves across a solid surface [19], which leads to a substantial velocity difference between the main front and the fluid on the micropillar. The dimensionless droplet diameter d grows with the increase of H for small liquid thicknesses, where the value of d becomes saturated until a

critical value of H_{cr} (= 2.5) is reached. This is explained by the diminishing influence of the upper plate as the fluid thickness grows.

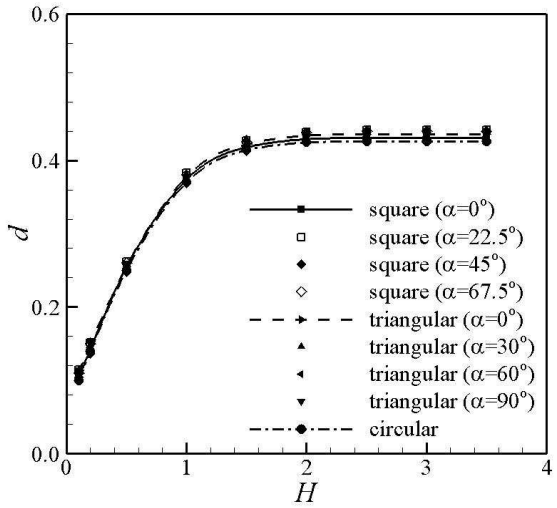

Figure 9 Dimensionless droplet diameter (d) as a function of H at Oh = 4.39×10^{-2} and Ca = 7.43×10^{-4}.

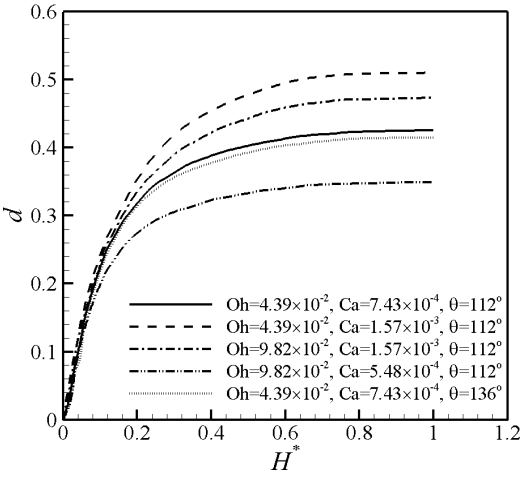

Figure 10 Calculation results of the dimensionless droplet diameter.

Figure 10 presents the theoretical calculation of the dimensionless droplet diameter expressed as a function of H^*, where $H^* = H/H_{cr}$. In the case of a fixed Ca and θ, the size of the droplet grows with the decrease of Oh. This can be

explained by the prevailing capillary effect on the surface at small Oh numbers, which dominates the front-moving process across the micropillar and leads to a growth of the droplet diameter. In cases of a fixed Ca and Oh, a large contact angle results in a large microdroplet due to the growth of the wetted surface on top of the micropillar. In the case of a fixed Oh and θ, the size of the droplet grows with the increase of Ca. When the value of Ca increases, the viscous force on the wetted surface, i.e. on the top surface of the micropillar, magnifies, which slows down the movement of the water front attached to the top surface of the micropillar. Thus, the capillary force is prone to create a microdroplet with a large diameter.

4 Conclusions

The influences of three different cross-sectional shapes and their orientation on microdroplet formation via a dewetting process were studied using a numerical approach. The numerical simulations show that the cross-sectional shape of a micropillar and their orientation give similar flow patterns, but have a nontrivial effect on the detachment time. The numerical results also indicate that the microdroplet diameter is almost insensitive to the cross-sectional shape and orientation of micropillars with the same size. The size of the droplets grows with the decrease of Oh, but reduces with the decline of Ca.

References

[1] Sugiura, S., Nakajima, M. & Seki, M., *Prediction of Droplet Diameter for Microchannel Emulsification*, Langmuir, **18**(10), pp. 3854-3859, 2002.

[2] Xu, J.H., Luo, G.S., Chen, G.G. & Wang, J.D., *Experimental and Theoretical Approaches on Droplet Formation from A Micrometer Screen Hole*, Journal of Membrane Science, **266**(1-2), pp. 121-131, 2005.

[3] Gupta, A. & Kumar, R., *Effect of Geometry on Droplet Formation in The Squeezing Regime in A Microfluidic T-Junction*, Microfluid Nanofluid, **8**(6), pp. 799-812, 2010.

[4] Luo, C., Xing, R., Zhang, Z., Fu, J. & Han, Y., *Ordered Droplet Formation by Thin Polymer Film Dewetting on A Stripe-Patterned Substrate*, Journal of Colloid and Interface Science, **269**(1), pp. 158-163, 2004.

[5] Yoon, B., Acharya, H., Lee, G., Kim, H., Huh, J. & Park, C., *Nanopatterning of Thin Polymer Films by Controlled Dewetting on A Topographic Pre-Pattern*, Soft Matter, **4**(1), pp. 1476-1472, 2008.

[6] Mulji, N. & Chandra, S., *Rupture and Dewetting of Water Films on Solid Surfaces*, Journal of Colloid and Interface Science, **352**(1), pp. 194-201, 2010.

[7] Zhang, Z., Wang, Z., Xing, R. & Han, Y., *How to Form Regular Polymer Microstructures by Surface-Pattern-Directed Dewetting*, Surface Science, **539**(1-3), pp. 129-136, 2003.

[8] Martin, C.P., Blunt, M.O., Vaujour, E.P., Stannard, A. & Moriarty, P., *Controlling Pattern Formation in Nanoparticle Assemblies via Directed Solvent Dewetting*, Physical Review Letters, **99**(11), 116103, pp. 1-4, 2007.

[9] Reiter, G., Al Akhrass, S., Hamieh, M., Damman, P., Gabriele, S., Vilmin, T. & Raphaël, E., *Dewetting as An Investigative Tool for Studying Properties of Thin Polymer Films*, The European Physical Journal Special Topics, **166**, pp. 165-172, 2009.

[10] Karthaus, O., Mikami, S. & Hashimoto, Y., *Control of Droplet Size and Spacing in Micrometer-Sized Polymeric Dewetting Patterns*, Journal of Colloid and Interface Science, **301**(2), pp. 703-705, 2006.

[11] Guan, J., Boukany, P.E., Hemminger, O., Chiou, N.R., Zha, W. & Lee, L.J., *Large Laterally Ordered Nanochannel Arrays from DNA Combing and Imprinting*, Advanced Materials, **22**(36), pp. 3997-4001, 2010.

[12] Lin, C.H., Guan, J., Chau, S.W., Chen, S.C. & Lee, L.J., *Patterning Nanowire and Micro-/Nanoparticle Array on Micropillar-Structured Surface: Experiment and Modeling*, Biomicrofluidics, **4**(3), 034103, pp. 1-15, 2010.

[13] Muzaferija, S., *Adaptive Finite Volume Method for Flow Prediction Using Unstructured Meshes and Multigrid Approach*, PhD Thesis, Department of Mechanical Engineering, University of London, 1994.

[14] Khosla, P.K. & Rubin, S.G., *A Diagonally Dominant Second-Order Accurate Implicit Scheme*, Computers and Fluids, **2**(2), pp. 207-209, 1974.

[15] Pantankar, S.V., *Numerical Heat Transfer and Fluid Flow*, 1st edition, Hemisphere, pp. 30-70, 1980.

[16] Lin, C.H., Guan, J., Chau, S.W. & Lee, L.J., *Experimental and Numerical Analysis of DNA Nanostrand Array Formation by Molecular Combing on Microwell Patterned Surface*, Journal of Physics D: Applied Physics, **42**(2), 025303, pp.1-8, 2009.

[17] Perić, M. & Ferziger, J.H., *Computational Methods for Fluid Dynamics*, 1st edition, Springer, 25-50, 1996.

[18] Dwiyantoro, B.A. & Chau, S.W., *The Dynamic Behavior of Droplet Formation on Micropillar Surface During A Dewetting Process*, 12th IEEE International Conference on Nanotechnology (IEEE-NANO), pp. 1-6, 2012.

[19] De Gennes, P.G., Brochard-Wyart, F. & Quéré, D., *Capillarity and Wetting Phenomena*, Springer, 2002.